Research in Astron. Astrophys. **2012** Vol. **12** No. **12**, 1701–1713
http://www.raa-journal.org *http://www.iop.org/journals/raa*

Research in Astronomy and Astrophysics

The impact of turbulence on electron heating and acceleration near the neutral point of externally driven reconnecting current sheets in solar flares *

Gui-Ping Wu[1], Hai-Sheng Ji[2] and Zong-Jun Ning[2]

[1] Department of Physics, Southeast University, Nanjing 210096, China; *wuguiping@seu.edu.cn*
[2] Purple Mountain Observatory, Chinese Academy of Sciences, Nanjing 210008, China

Received 2012 March 9; accepted 2012 June 1

Abstract We aim to investigate the influence of plasma instability on electron acceleration and heating near the neutral point of a turbulent reconnecting current sheet (RCS). Through numerically solving the one dimensional relativistic Vlasov equation with typical solar coronal parameters and a realistic mass ratio in the presence of a strong inductive electric field E_0, we suggest that the wave-particle scattering may produce a flat electron flux spectrum from thermal to nonthermal electrons without a sudden low-energy cutoff in the acceleration region. The ratio between electron heating and acceleration decreases with the increase of the induced electric field. It is about one for E_0=1 V cm^{-1} and one fourth for E_0=10 V cm^{-1}. The unstable waves excited by the beam plasma instability first accelerate the electrons, then trap these electrons from further acceleration by an induced electric field through wave-particle resonant interactions.

Key words: turbulence — scattering — Sun: X-rays, gamma rays — acceleration of particles

1 INTRODUCTION

In solar flares, the temporal evolution of the energetic electrons may be inferred from hard X-ray (HXR) and microwave emissions. Their distribution is usually described by a power law with a low-energy cutoff in the range of 20–40 keV (Brown 1971; Benka & Holman 1994; Dennis et al. 2003; Holman 2003; Sui et al. 2004; Huang et al. 2005; Huang 2009; Sui et al. 2007; Kontar et al. 2008). Recently, Hannah et al. (2009) argued that, when these energetic electrons are transported down into the low corona, they first excite Langmuir waves, and then react to the energetic electron beam. Finally, the positive distribution of the energetic electrons is formed below the low cutoff energy and down to the thermal energies. Therefore, they suggested that a flat spectrum (spectral index of 0–1) below the low cutoff energy and down to thermal energies may be a better approximation instead of a sharp cutoff in the injected electron spectrum.

On the other hand, magnetic reconnection is generally accepted to be the prime mechanism that turns the free magnetic energy into heating and accelerating electrons in solar flares. A series of

* Supported by the National Natural Science Foundation of China.

work has been devoted to investigate the temporal correlation between the reconnection rate, i.e., the induced electric field strength on the order of about $1 \sim 10$ V cm^{-1}, and the total flux and spectral index of HXR emissions, where the reconnection rate is calculated from the flare ribbon separation speed and the photospheric magnetic field; the corresponding reconnection rate is about 0.005$\sim$0.05 with a coronal density of $10^{14} - 10^{16}$ m^{-3} and a magnetic field strength of 100 G (Poletto & Kopp 1986; Forbes & Lin 2000; Lin et al. 2003; Jing et al. 2005; Liu et al. 2008; Liu & Wang 2009; Yang et al. 2011 and references therein). It has been found that the induced electric field strength exhibits a positive correlation with the total HXR flux, and a negative correlation with the HXR spectral index in the impulsive phase of solar flares. These results strongly suggest that the particles are accelerated to higher energies by larger reconnecting electric fields, and then precipitate into the lower chromosphere to produce stronger HXR emissions. In particular in the Earth's magnetotail, energetic electrons up to $\sim$ 300 keV were directly measured in a rare crossing of the diffusion region of the reconnecting current sheet (RCS) by the Wind spacecraft and Cluster (Øieroset et al. 2002; Wang et al. 2010a,b,c). Egedal et al. (2010), after analyzing in-situ measurements of electron distribution functions inside the magnetotail RCS from Wind and Cluster, found that the relative energy gain of the super-thermal electrons is the same and nearly independent of their initial energy, while electrons with the thermal energy are less accelerated. Huang et al. (2010) also found that electrons with thermal energy are less accelerated in their 2D particle-in-cell (PIC) simulations. Hence, they concluded that the super thermal electrons are accelerated by the reconnecting parallel electric field in the vicinity of the reconnection region. For other acceleration mechanisms, such as Fermi acceleration of electrons in contracting magnetic islands and stochastic acceleration, the relative energy gain of the electrons is a function of their initial energy (Miller et al. 1997; Aschwanden 2002; Drake et al. 2006). Therefore, these direct observational signatures further suggest that the electrons are accelerated to relativistic energy by the reconnecting electric field inside the diffusion region near the neutral point.

Theoretically, as the reconnecting electric field is much larger than the classical Drecier value during the eruptive phase of solar flares and in the Earth's magnetotail (Martens & Young 1990), the bulk of electrons are freely accelerated near the center of the RCS before the unstable waves are excited. With different prescribed electromagnetic fields in the RCS, the equation of motion for a single particle was solved analytically or by test particle simulations, but the electromagnetic fields induced by the accelerated particles were ignored for more than four decades (Speiser 1965; Martens & Young 1990; Litvinenko 1996, 2000; Onofri et al. 2006; Liu et al. 2009). It is found that the acceleration time is limited by the ratio of the guiding field component to the transverse component of the magnetic field (see eq. 40 of Litvinenko 1996), the energetic electrons follow a power-law distribution, and the spectral index mainly depends on the magnetic configuration (Litvinenko 1996, 2000; Wu et al. 2005). Recently, the electron dynamics inside the ion diffusion region of the RCS and the macroscopic magnetic reconnection were also investigated with the reduced mass ratio and unrealistic parameters in 2D and 3D PIC and MHD simulations (Hoshino et al. 2001, Fu et al. 2006, Pritchett 2006; Daughton et al. 2009, 2011; Huang & Bhattacharjee 2010; Cassak & Shay 2011 and references therein). It is shown that: (1) with the guiding magnetic field or externally driven reconnection, the electrons are mainly accelerated by the reconnecting electric field in the X-type region, then spread out along the separatrices, and no obvious electron acceleration is observed in the O-type region; (2) without the guiding magnetic field, the electrons are accelerated not only around the X-type region due to the meandering motion but also near the region showing magnetic-field pileup due to the ∇B drift and the curvature drift; (3) the large scale RCS breaks into a number of secondary magnetic islands with the scale of ion inertial length for the Lundquist number above 10^4 due to the tearing instability, and the reconnection rate is about $0.01\sim 0.1$ and is not dependent on the Lundquist number. The free magnetic energy is then transferred into the accelerating electrons by the direct electric field along the x line and merging points of the multi-island coalescences, i.e., anti-reconnection (Pritchett 2008; Oka et al. 2010).

Previously, we carried out one dimensional (1D) non-relativistic self-consistent Vlasov simulations using the Vlasov equation, including the external inductive field with a realistic mass ratio and typical coronal parameters for the first time, investigated the characteristics of the excited electrostatic waves, and deduced the dependence of anomalous resistance on the external inductive field and the bulk drift velocity (Wu & Huang 2009; Wu et al. 2010a,b). We clarified that, owing to the presence of a super-Dreicer electric field, the bulk drift velocity increases beyond the threshold of Buneman instability (Buneman 1959), which can be quickly excited. With the deviation of the electron distribution from being Maxwellian, more unstable waves are excited. The larger the electric field strength is, the higher the turbulence level is (Wu & Huang 2009). In the previous simulations, as the sum of the means ($v_{\rm d}$) and the standard deviations ($v_{\rm e}$) of the electron velocity v_z is always less than $0.1c$, the non-relativistic approximation is plausible (refer to fig. 2 of Wu & Huang 2009). However, if we investigate the electron heating and acceleration near the X-type neutral point of the RCS, the simulation time is longer and the maximum electron velocity approaches light speed, so the relativistic effect should be taken into account.

In the present work, we numerically solve the relativistic Vlasov equation with a large induced electric field, further investigate the impact of unstable waves on electron heating and acceleration near the null point of the turbulent RCS, and pay more attention to the impact of unstable waves on the low energy electrons. The basic equation and simulation method are described in Section 2. The unstable wave-particle interaction, the electron heating and acceleration, the nonlinear dependence of the anomalous resistivity and the spectra of the unstable waves on the induced electric field are presented in Section 3. The discussion and conclusion are provided in Section 4.

2 BASIC EQUATION AND SIMULATION METHOD

As stated above, the electrons are most effectively accelerated to relativistic energies near the centerplane of a current sheet near the X-type point, where the induced electric field is assumed to be along the z-component of the magnetic field (guiding field), the other two components of the magnetic field approach zero, and the Lorentz force ($\boldsymbol{J}\times\boldsymbol{B}$) is smaller than the electric force (Øieroset et al. 2002; Watt et al. 2002; Omura et al. 2003; Pritchett 2006; Fu et al. 2006; Petkaki & Freeman 2008; Wu & Huang 2009). Therefore, a 1D approach is used to investigate the heating and acceleration of electrons in the RCS as before (Boris et al. 1970; Petkaki & Freeman 2008; Wu & Huang 2009).

The 1D electrostatic relativistic Vlasov equation is written as (Suzuki & Shigeyama 2010)

$$\frac{\partial f_\alpha}{\partial t}+\frac{p_z}{\gamma m_\alpha}\frac{\partial f_\alpha}{\partial z}+q_\alpha E_z\frac{\partial f_\alpha}{\partial p_z}=0, \tag{1}$$

where f_α is the particle distribution function ($\alpha\in\{i,e\}$), $p_z=\gamma m_\alpha v_z$ is the momentum of particles, $\gamma=1/\sqrt{1-v_z^2/c^2}$ is the Lorentz factor (for ions, the relativistic effect may be ignored, i.e., $\gamma=1$), c is the speed of light, m_α and q_α are respectively the mass and charge of the particles, and E_z is the electric field strength, including the inductive component E_0 and turbulent component $\widehat{E}$, i.e., $E_z=E_0+\widehat{E}$. The former is assumed to be a constant in time and space, and the latter may be integrated forward in time, using Ampere's law given by (Horne & Freeman 2001)

$$(\nabla\times\boldsymbol{B})_z=\mu_0(J+\varepsilon_0\frac{\partial E_z}{\partial t}). \tag{2}$$

The electric current density is expressed by

$$J(z,t)=\sum q_\alpha\int\frac{p_z}{\gamma m_\alpha}f_\alpha(z,p_z,t)dp_z, \tag{3}$$

which may also be divided into two parts of a spatially-averaged component $\langle J\rangle$ and a fluctuating component $\widehat{J}$, i.e., $\widehat{J}=J-\langle J\rangle$.

Table 1 Summary of Simulation Parameters

Parameter	Symbol	Value
Ion to electron mass ratio	m_p/m_e	1836
Plasma density	$n = n_\mathrm{i} = n_\mathrm{e}$	10^{14} m^{-3}
Temperature	$T = T_\mathrm{e} = T_\mathrm{i}$	10^7 k
Initial drift momentum	p_d	$1.5 m_\mathrm{e} v_\mathrm{e0}$
Induced electric field strength	E_0	$1 \sim 10$ V cm^{-1}
Number of spatial grid points	N_z	2000
Number of velocity grid points	$N_\mathrm{pe}, N_\mathrm{pi}$	$2500 \sim 3000, 400$
Resolution of the spatial grid	Δz	$0.5\lambda_\mathrm{De}$
Resolution of the velocity grid	$\Delta p_\mathrm{e}, \Delta p_\mathrm{i}$	$0.015 m_\mathrm{e} v_\mathrm{e0}, 0.05 m_\mathrm{i} v_\mathrm{i}$
Resolution of time	Δt	$0.002 \sim 0.004 w_\mathrm{pe}^{-1}$

Because we investigate plasma waves at small scales and at high frequencies (typical for coronal plasma), the first order approach is usually adopted. To extend Equation (2) to first order, $\mu_0 < J >$ is balanced by the gradient of an external magnetic field $\boldsymbol{B}$ at all times, i.e., $(\nabla \times \boldsymbol{B})_z = \mu_0 \langle J \rangle$ (Omura et al. 1996; Watt et al. 2002), and $\widehat{J}$ is related to the displacement current, i.e, $\widehat{J} = -\varepsilon_0 \frac{\partial \widehat{E}}{\partial t}$, which is a small correction to $\langle J \rangle$ (about three orders less than $\langle J \rangle$ in our simulations). The anomalous resistivity may be calculated by (Wu et al. 2010a)

$$\eta_\mathrm{eff} = \frac{E_0}{\langle J \rangle} - \frac{m_\mathrm{e}}{n_\mathrm{e} e^2} \left(\frac{1}{\langle J \rangle} \frac{d\langle J \rangle}{dt} \right). \tag{4}$$

We adopt a system of normalized units where mass is normalized to the electron mass m_e, velocity to the speed of the initial electron thermal velocity v_e0, time to the inverse electron plasma frequency ω_pe^{-1}=1.773 $\times$ 10^{-9} s, and distance to the electron Debye length $\lambda_\mathrm{De} = v_\mathrm{e0}/\omega_\mathrm{pe}$ ($v_\mathrm{e0} = \sqrt{kT_\mathrm{e}/m_\mathrm{e}}$, k is the Boltzmann constant). Correspondingly, the Lorentz factor is $\gamma = \sqrt{1 + \alpha^2 p^2}$, where $\alpha = v_\mathrm{e0}/c$, $p = p_z/m_\mathrm{e}/v_\mathrm{e0}$.

With the periodic boundary conditions and second order MacCormack finite difference in time and space described in Horne & Freeman (2001), Equation (1) is integrated forward in time, with initial unstable waves originating in a white noise electric field applied at $t = 0$ (see eqs. (4) and (5) in Petkaki et al. 2003). The initial ion and electron populations are uniform in space and Maxwellian in velocity space, drifting to each other, i.e.,

$$\begin{aligned} f_\mathrm{i}(p_z) &= n/((2\pi)^{1/2} v_\mathrm{i}) \exp(-p_z^2/(2p_\mathrm{i}^2)), \\ f_\mathrm{e}(p_z) &= n/((2\pi)^{1/2} v_\mathrm{e0}) \exp(-(p_z - p_\mathrm{d})^2/(2p_\mathrm{e}^2)), \end{aligned}$$

where $v_\mathrm{i} = \sqrt{kT_\mathrm{i}/m_\mathrm{i}}$ is the ion thermal velocity and $p_\mathrm{i} = m_\mathrm{i} v_\mathrm{i}$ is the ion thermal momentum. The simulation parameters are summarized in Table 1, where the space, momentum space, and time numbers of grid points are carefully selected to ensure the numerical stability and accuracy of the integration algorithm (Horne & Freeman 2001; Petkaki et al. 2003).

3 ELECTRON HEATING AND ACCELERATION NEAR THE NULL POINT OF RCS

3.1 Evolution of the Electron Distribution

After numerically solving Equations (1)–(3), we present the electron distribution averaged along the z-axis, with or without the turbulent component of the electric field in Figure 1 for $E_0 = 8$ V cm^{-1}. It is shown from Figure 1(a) that, when the turbulent component $\widehat{E} = 0$, the bulk of electrons are freely accelerated and the single drift Maxwellian distribution appears. From Figure 1(b) and (c), we see that, when the turbulent component of the electric field is considered, the distribution

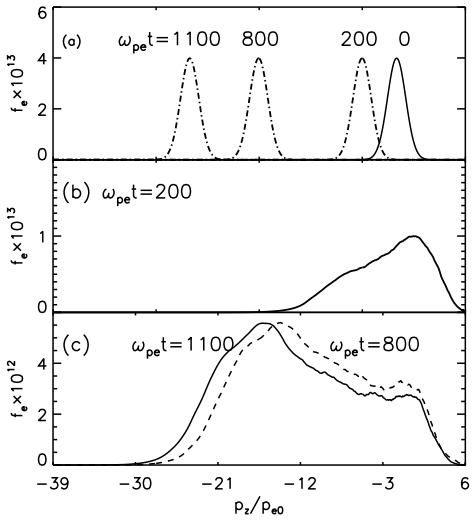

Fig. 1 The time dependent distribution of electrons for an induced electric field strength of 8 V cm^{-1} without the turbulent component of the electric field in (a), and with the turbulent component of the electric field in (b)–(c).

deviates from being Maxwellian. At the beginning, the electrons show bulk drift before the unstable waves are excited to some level. Then, when the magnitude of unstable waves increases and they influence energetic electrons, those electrons with high velocity are dragged to the low-velocity regime. Finally, those electrons trapped by waves stop accelerating, but untrapped electrons continue to be accelerated. If we compare Figure 1(a) and (b) in the high momentum regime between –16.5 and –5.3 at $\omega_{\rm pe}t = 200$, these electrons are accelerated by the wave-particle resonant interaction rather than by the induced electric field. From Figure 1(a) and (c), we may also see that the energetic electrons near a momentum of 25 are accelerated first by turbulent waves at $\omega_{\rm pe}t = 800$ and then are trapped from further acceleration by the induced electric field at $\omega_{\rm pe}t = 1100$. This will be explained with the following spectral analysis of unstable waves (see Sect. 3.5).

3.2 Electron Heating and Acceleration

In order to further investigate the influence of turbulence on electron acceleration by the induced electric field in the RCS, we plot their evolution in the spatially averaged density of the turbulent energy $\sigma_E = \frac{\varepsilon_0 \hat{E}^2}{2n_{\rm e}kT}$, the spatially averaged mean drift momentum $p_{\rm d}/p_{\rm e0}$, the rms deviation from mean momentum $p_{\rm e}/p_{\rm e0}$, the freely accelerated momentum of electrons, and the ratio of $p_{\rm d}/p_{\rm e}$ versus time in Figure 2 for $E_0 = 1$ V cm^{-1} and Figure 3 for $E_0 = 10$ V cm^{-1}. It is shown from Figure 2 that the whole evolution can be described as follows. At the beginning, the electrons are all freely accelerated by the induced electric field. Secondly, the unstable waves increase exponentially and react to energetic electrons. The drift velocity decreases and the random velocity increases. Thirdly, after the instability saturates, the untrapped electrons continue to be accelerated. The bulk drift velocity continues to rise and the unstable waves increase again, and the above process repeatedly occurs.

From Figure 2(c), we see that $p_{\rm d}/p_{\rm e} \approx 1$, which suggests that the heating and acceleration rates are almost the same and half of the released energy goes into heating electrons, i.e., $\frac{p_{\rm d}^2}{2m_{\rm e}} \approx \frac{p_{\rm e}^2}{2m_{\rm e}}$. With the increase of the induced electric field strength from 1 V cm^{-1} to 10 V cm^{-1}, the averaged

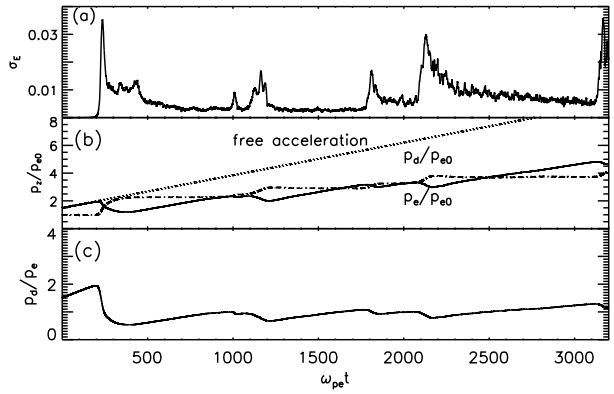

Fig. 2 Evolution in the fluctuating electric field energy (a), bulk drift velocity, thermal velocity, and freely accelerated velocity of electrons (b), and the ratio of the bulk drift velocity to thermal velocity (c) for the induced electric field strength of 1 V cm^{-1}.

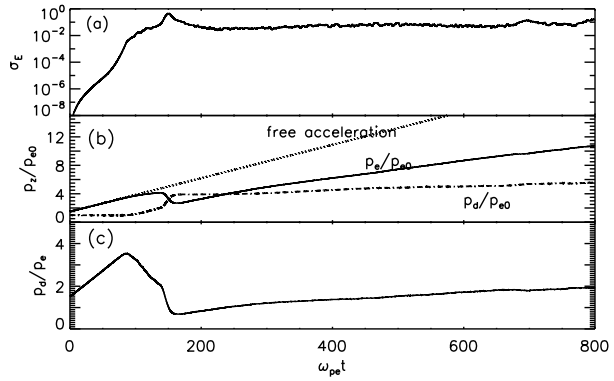

Fig. 3 Evolution in the fluctuating electric field energy (a), bulk drift velocity, thermal velocity, and freely accelerated velocity of electrons (b), and the ratio of the bulk drift velocity to thermal velocity (c) for the induced electric field strength of 10 V cm^{-1}.

ratio between heating and acceleration decreases from about 1 to 0.25 (see Figs. 2(c) and 3(c)). The higher E_0 is, the more efficient acceleration is.

3.3 Influence of Turbulence on Low-energy Electrons Accelerated by the Induced Electric Field

Strictly speaking, the energetic electron spectrum can be obtained only when the 3D3V Vlasov simulations are performed. However, due to the limitations of calculation ability, different approaches are adopted in the present simulations. As the electrons are most efficiently accelerated near the neutral point and then eject out along the magnetic separatrices with little change of their energy (Fu et al. 2006), we may investigate the influence of turbulence on the low-energy electrons accelerated by the induced electric field near the neutral point of the RCS.

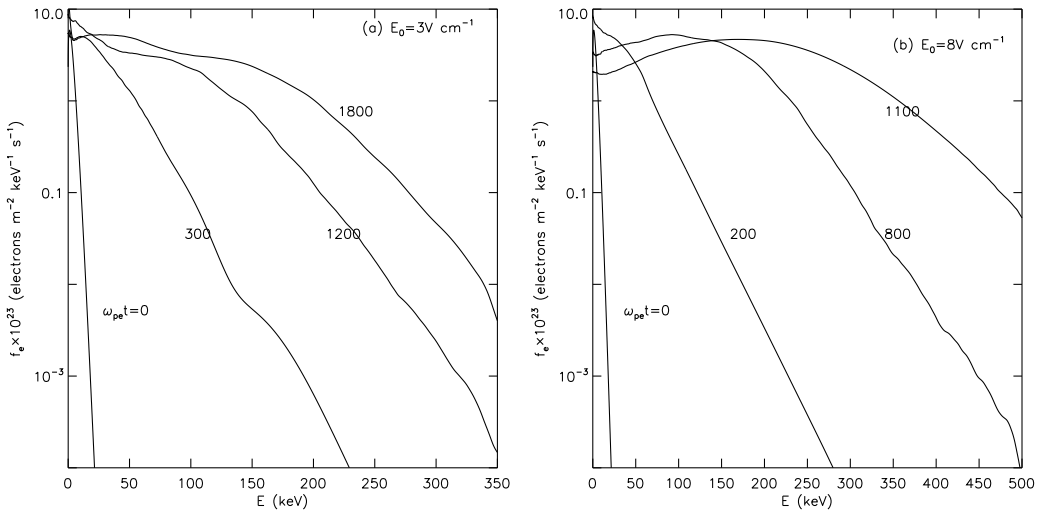

Fig. 4 Time dependent spectrum of energetic electrons for the induced electric field strength of 3 V cm^{-1} and 8 V cm^{-1}.

The electron flux spectrum $f(E,t)$ may be inferred from electron distribution $f(p,t)$. With kinetic energy $E=(\gamma-1)m_{\rm e}c^2=(\sqrt{1+\alpha^2p^2}-1)m_{\rm e}c^2$, we have $f(E,t)=\frac{p_z}{\gamma m_{\rm e}}\frac{\partial p}{\partial E}f(p,t)=f(p,t)/m_{\rm e}/v_{\rm e0}$. The time dependent $f(E,t)$ is shown in Figure 4. It is seen that the electron flux from the thermal to nonthermal regime changes smoothly without a sudden low-energy cutoff. Considering the energetic electrons ejected out of the contributions from the different acceleration time and induced electric field, we argue that the turbulent waves play an important role and form a flat flux in a low-energy regime. Of course, this theory requires multidimensional high resolution simulations for confirmation.

It is well known that in the impulsive phase of solar flares the energetic electrons are usually assumed to follow a power-law with a low-energy cutoff and without any theoretical explanation. The low-energy cutoff is a key parameter in the calculation of nonthermal electron energy (Holman 2003). Our simulations may help to understand the different low-energy cutoffs in different events with a different reconnecting electric field (Benka & Holman 1994; Gan et al. 2001; Sui et al. 2004; Huang et al. 2005; Huang 2009).

3.4 Anomalous Resistivity

Previously, we have investigated the nonlinear dependence of the anomalous resistivity on the induced electric field and bulk drift velocity in the nonrelativistic 1D1V Vlasov simulations with real solar coronal parameters and the mass ratio of electrons to protons (Wu et al. 2010a,b). As the relativistic correction is taken into account in the present paper, we can study the evolution of the electron distribution in the typical characteristic time of acceleration by the induced electric field. The smaller E_0 is, the longer the calculation time will be. We work out the dynamic changes of the anomalous resistivity according to Equation (4) for different E_0 (see Fig. 5). It is shown in Figures 2 and 5(a) that for each excitation of unstable waves the bulk drift energy is quickly transferred into random energy, and the anomalous resistivity increases. When the waves saturate, the energy between the waves and electrons exchanges stochastically, i.e., the averaged bulk drift momentum increases fast, caused by the induced electric field, while the random momentum is almost unchanged. Correspondingly, the

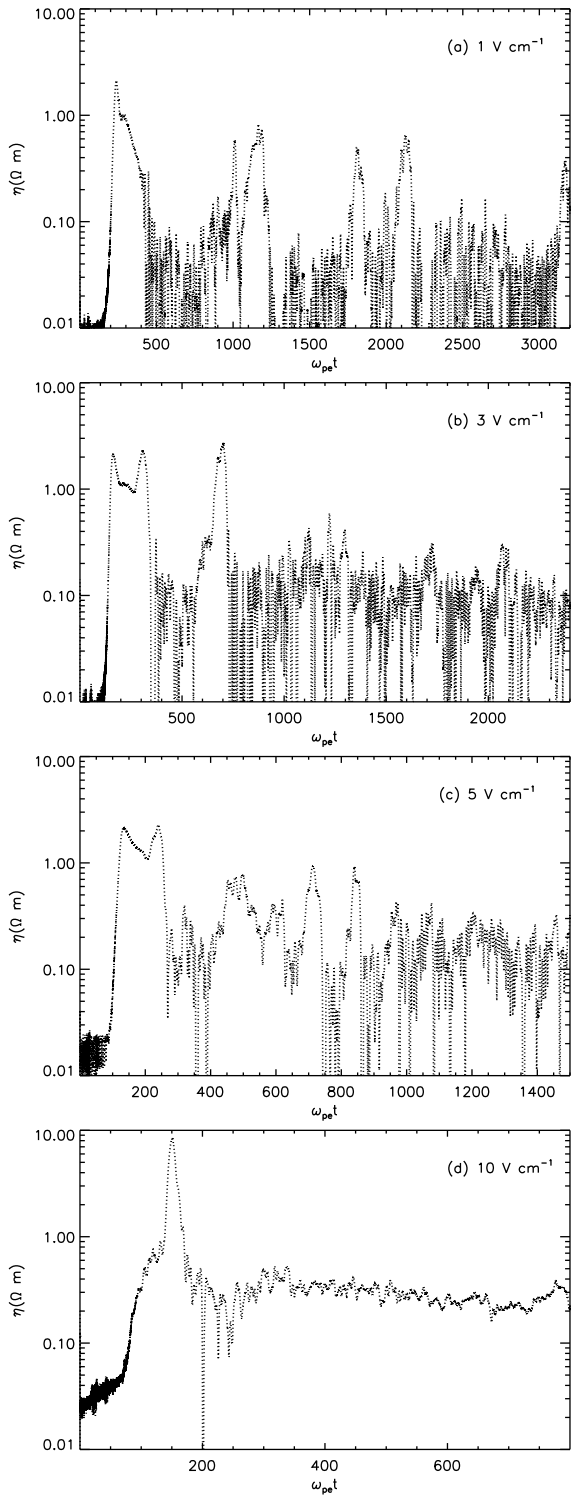

Fig. 5 Evolution of anomalous resistivity as a function of the induced electric field.

anomalous resistivity is sometimes positive and sometimes negative. From Figure 3 and Figure 5(d), we can see that the anomalous resistivity is almost positive, which implies that the energetic electrons transfer their energy into waves, then the waves transfer energy into the random motion of electrons. Therefore, the bulk drift velocity increases less than the free acceleration and the random momentum is slowly enhanced (Fig. 3(b)). This means that it is implausible for the bulk drift velocity to be the only variable in the formula of anomalous resistivity in MHD simulations (Yokoyama & Shibata 1994).

3.5 Dispersion Relation

In order to understand the nonlinear characteristics and the dispersion relationship of the unstable electrostatic waves, the spectra of the turbulent electric field in the $k-\omega$ space are shown in Figure 6 for $E_0 = 1$ V cm^{-1} and Figure 7 for $E_0 = 8$ V cm^{-1}. It may be seen from Figures 2(b) and 6 that with every excitation of unstable waves, the low-frequency branch propagates mainly along the z-axis direction with a frequency on the order of $\omega_{\rm pi}$ and the phase velocity is less than the electron thermal velocity. The high-frequency branch of unstable waves propagates in the opposite direction along the z-axis with a phase velocity in the regime of about $1.5 \sim 5\ v_{\rm e0}$ and a frequency from 0 to 2 $\omega_{\rm pe}$, which is excited by the beam-plasma instabilities due to the deviation of the electron distribution from being Maxwellian. It is from the reaction of these waves that the high energy electrons are dragged to low energy ones to form the low energy tail that does not experience further acceleration.

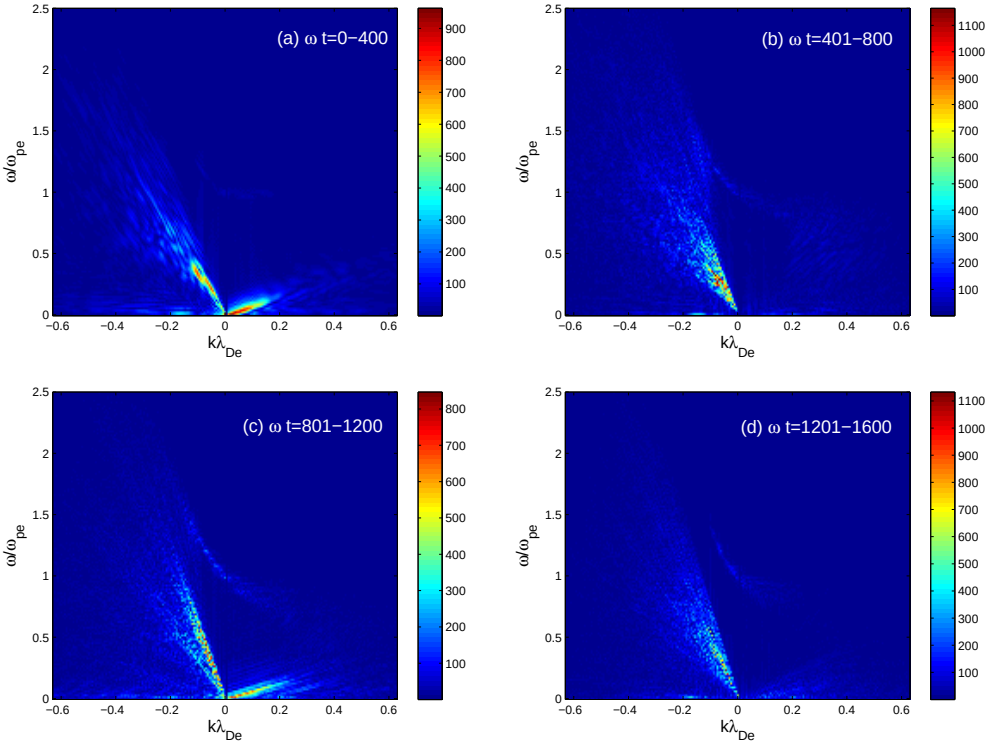

Fig. 6 Turbulent electric field spectra obtained by Fourier transformation with the induced electric field of 1 V cm^{-1}.

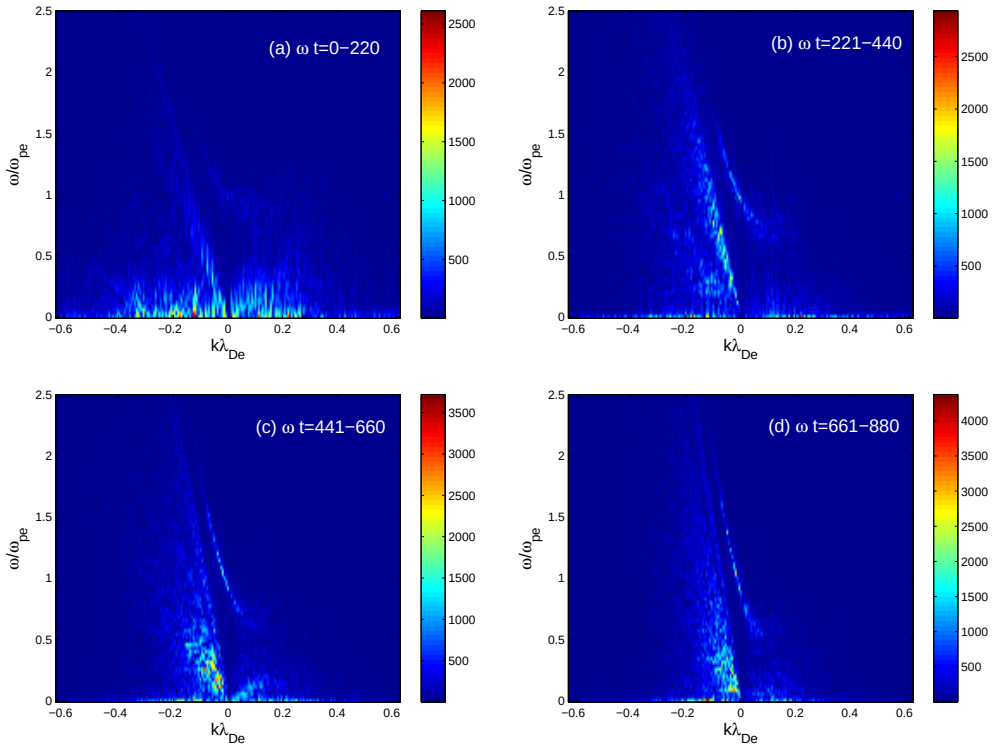

Fig. 7 Turbulent electric field spectra obtained by Fourier transformation with the induced electric field of 8 V cm^{-1}.

For $E_0 = 8$ V cm^{-1}, the spectra of the turbulent electric fields (Fig. 7) are slightly different from those in Figure 6. The low-frequency waves always propagate bi-directionally. The two high-frequency branches of unstable waves are excited with phase velocity of several times to tens of the initial thermal velocity. This can be used to interpret the electron distribution in Figure 1. At first, wave-particle resonant interaction accelerates the electrons near the phase velocity due to the positive distribution of electrons (the number of electrons increase with the decrease of the momentum), then traps these electrons from further acceleration by the induced electric field due to quasi platform distribution.

4 DISCUSSIONS AND CONCLUSIONS

The primary purpose of this paper is to investigate the role of unstable waves on electron heating and acceleration near the neutral point of the turbulent RCS. A simplified 1D1V relativistic Vlasov simulation with realistic plasma parameters is used to get some insight into the physical nature of the low-energy electron distribution and process of electron heating and acceleration. As $B_x = B_y \approx 0$ is assumed, the spatial scale of calculation may be estimated as

$$L_x \times L_y \times L_z = c/\omega_{\rm pi} \times c/\omega_{\rm pe} \times L_z \,,$$

where $\omega_{\rm pi}$, $\omega_{\rm pe}$ and L_z are respectively the ion plasma frequency, the electron plasma frequency and the macroscopic length along the guiding field (as the periodic boundary condition is used in this direction).

In principle, the acceleration of the externally driven RCS with a guiding magnetic field should be investigated in the 3D3V numerical simulations with real physical parameters on a macroscopic scale. Due to the limitation of available computing power, the higher the dimension is, the lower the resolution of the grid points will be. Therefore, different approximations are taken in order to model different aspects of the physical nature. For example, in 2D simulations, a uniform distribution is widely adopted in the out-of-plane direction of the RCS, which may be improper as the electrostatic wave along the guiding field (the direction of the current) is not taken into account. In addition, though the reduced mass ratio and unrealistic parameters in 2D and 3D PIC simulations would save computing time, it may give an unreliable time-evolution of the considered process and an unreliable estimation of the order of the physical parameters (Hellinger et al. 2004).

Recently, Drake and his colleagues performed 3D PIC simulations and investigated the instability excited by the initial drift in a Maxwellian distribution of electrons with a strong guide field and unrealistic parameters in the dissipation region of double current sheets (Drake et al. 2003; Che et al. 2009, 2010). They illustrated that the parallel Buneman instability first grows and traps low velocity electrons, then the parallel electron-electron two-streaming instability and nearly-perpendicular lower hybrid instability grow. By stacking cuts of the parallel turbulent electric field, they demonstrated that the parallel phase velocity of unstable waves increases, which was used to explain that an electron with a high velocity was dragged to a lower velocity through wave-particle interactions (Che et al. 2009). Perhaps due to the intrinsic noise of PIC simulations, Che et al. (2009) did not provide dispersion of unstable waves. Vlasov simulations do not suffer from such noise, and may describe wave-particle resonances and particle acceleration in detail (Schmitz & Grauer 2006).

On the other hand, anomalous resistivity is always associated with microspace, i.e., a typical plasma scale such as electron inertial length and cyclotron radius. The magnetic reconnection takes place in macrospace. How to bridge these two space scales in the same framework is still an open question. Some important progress has been achieved by numerical simulations, laboratory experiments and in situ observations by satellites (see reviews by Yamada 2011 and Cassak & Shay 2011 and references therein). The main theory is that due to tearing instability, the large-scale RCS breaks into multiple islands with a scale of the inertial length of ions. The free magnetic energy is then transferred into accelerating electrons by a direct electric field in the x line and merging points of the multi-island coalescences (Drake et al. 2006; Pritchett 2008; Oka et al. 2010). Also, the merging of plasmoids and fragmentation was used to explain the drifting pulsating structure in the solar microwave band (Kliem et al. 2000) and above-loop-top HXR sources from the 2007 December 31 solar flare (Karlický & Bárta 2011). Bemporad (2008) considered that, because of the tearing and coalescence instability, many microscopic current sheets (CSs) inside the turbulent post CME-CS are formed and these could explain not only the high CS temperatures but also the much larger observed thickness of macroscopic CSs. In addition, Vlahos et al. (2004) suggested that particles are accelerated in an evolving network of unstable CSs. Acceleration and energy dissipation are assumed to be present in a large number of correlated RCSs.

Our simulations indicate that the unstable waves change the distribution of electrons, heating and accelerating electrons near the neutral point of the RCS. The main results are summarized as follows.

(1) When the ratio of the bulk drift velocity to random velocity reaches Buneman instability, the low frequency and low phase-velocity waves are excited and trap the low energy electrons, to stop them from accelerating. After the electron distribution deviates from being Maxwellian, the beam-plasma instability occurs. The phase-velocity of these unstable waves is from above $-v_{e0}$ to less than $-30v_{e0}$ and depends on the strength of the electric field. Due to the wave-particle resonant and nonresonant interaction, the waves with a phase-velocity of $(-1\sim-5)v_{e0}$ trap electrons to form a low energy tail; these waves with a phase-velocity on the order of

tens of the thermal velocity first accelerate electrons, and then trap these electrons from further acceleration by the induced electric field.

(2) The wave-particle scattering produces the flat electron flux spectrum from the thermal to non-thermal regime without a sudden low-energy cutoff in the acceleration region, which is important for estimating the energy budget and fitting the HXR spectrum in the solar flare.

(3) For $E_0 = 1$ V cm^{-1}, the heating and acceleration rate is almost the same. When E_0 increases, the acceleration rate increases, but the heating rate decreases. If the final bulk drift approaches the same value for different E_0, the number of times for the repeated excitation of unstable waves is enhanced with a decrease of E_0, and at the same time the bulk drift movement quickly transfers into random movement.

(4) As long term evolution of anomalous resistivity continues, it increases each excitation of unstable waves, so the bulk drift kinetic energy is quickly transferred into random energy. When the waves saturate for $E_0 = 1$ V cm^{-1}, the waves and electrons exchange energy stochastically, and the random momentum almost remains constant. The anomalous resistivity is sometimes positive and sometimes negative. For E_0=10 V cm^{-1}, the energy of the high energy electrons becomes wave energy, and then the wave energy is transferred into random motion of electrons and the random momentum is slowly enhanced. The anomalous resistivity is always positive. Such evolution of the anomalous resistivity should be taken into account in future MHD simulations.

Acknowledgements We are grateful to the referee for his constructive comments and suggestions on our work and manuscript. This study is supported by the National Natural Science Foundation of China (Grant Nos. 11073006 and 10833007). We would like to acknowledge the computational resources provided by the Department of Physics, Southeast University.

References

Aschwanden, M. J. 2002, Space Sci. Rev., 101, 1
Bemporad, A. 2008, ApJ, 689, 572
Benka, S. G., & Holman, G. D. 1994, ApJ, 435, 469
Boris, J. P., Dawson, J. M., Orens, J. H., & Roberts, K. V. 1970, Physical Review Letters, 25, 706
Brown, J. C. 1971, Sol. Phys., 18, 489
Buneman, O. 1959, Physical Review, 115, 503
Cassak, P. A., & Shay, M. A. 2011, Space Sci. Rev., 265 (doi 10.1007/s11214-011-9755-2)
Che, H., Drake, J. F., Swisdak, M., & Yoon, P. H. 2009, Physical Review Letters, 102, 145004
Che, H., Drake, J. F., Swisdak, M., & Yoon, P. H. 2010, Geophys. Res. Lett., 37, L11105
Daughton, W., Roytershteyn, V., Albright, B. J., et al. 2009, Physical Review Letters, 103, 065004
Daughton, W., Roytershteyn, V., Karimabadi, H., et al. 2011, Nature Physics, 7, 539
Dennis, B. R., Veronig, A., Schwartz, R. A., et al. 2003, Advances in Space Research, 32, 2459
Drake, J. F., Swisdak, M., Cattell, C., et al. 2003, Science, 299, 873
Drake, J. F., Swisdak, M., Che, H., & Shay, M. A. 2006, Nature, 443, 553
Egedal, J., Lê, A., Zhu, Y., et al. 2010, Geophys. Res. Lett., 37, L10102
Forbes, T. G., & Lin, J. 2000, Journal of Atmospheric and Solar-Terrestrial Physics, 62, 1499
Fu, X. R., Lu, Q. M., & Wang, S. 2006, Physics of Plasmas, 13, 012309
Gan, W. Q., Li, Y. P., & Chang, J. 2001, ApJ, 552, 858
Hannah, I. G., Kontar, E. P., & Sirenko, O. K. 2009, ApJ, 707, L45
Hellinger, P., Trávníček, P., & Menietti, J. D. 2004, Geophys. Res. Lett., 31, L10806
Holman, G. D. 2003, ApJ, 586, 606
Horne, R. B., & Freeman, M. P. 2001, Journal of Computational Physics, 171, 182
Hoshino, M., Mukai, T., Terasawa, T., & Shinohara, I. 2001, J. Geophys. Res., 106, 25979

Huang, C., Lu, Q., & Wang, S. 2010, Physics of Plasmas, 17, 072306
Huang, G. 2009, Sol. Phys., 257, 323
Huang, G., Zhou, A., Su, Y., & Zhang, J. 2005, New Astron., 10, 219
Huang, Y.-M., & Bhattacharjee, A. 2010, Physics of Plasmas, 17, 062104
Jing, J., Qiu, J., Lin, J., et al. 2005, ApJ, 620, 1085
Karlický, M., & Bárta, M. 2011, ApJ, 733, 107
Kliem, B., Karlický, M., & Benz, A. O. 2000, A&A, 360, 715
Kontar, E. P., Dickson, E., & Kašparová, J. 2008, Sol. Phys., 252, 139
Lin, R. P., Krucker, S., Hurford, G. J., et al. 2003, ApJ, 595, L69
Litvinenko, Y. E. 1996, ApJ, 462, 997
Litvinenko, Y. E. 2000, Sol. Phys., 194, 327
Liu, C., Lee, J., Jing, J., Gary, D. E., & Wang, H. 2008, ApJ, 672, L69
Liu, C., & Wang, H. 2009, ApJ, 696, L27
Liu, W. J., Chen, P. F., Ding, M. D., & Fang, C. 2009, ApJ, 690, 1633
Martens, P. C. H., & Young, A. 1990, ApJS, 73, 333
Miller, J. A., Cargill, P. J., Emslie, A. G., et al. 1997, J. Geophys. Res., 102, 14631
Øieroset, M., Lin, R. P., Phan, T. D., Larson, D. E., & Bale, S. D. 2002, Physical Review Letters, 89, 195001
Oka, M., Phan, T.-D., Krucker, S., Fujimoto, M., & Shinohara, I. 2010, ApJ, 714, 915
Omura, Y., Matsumoto, H., Miyake, T., & Kojima, H. 1996, J. Geophys. Res., 101, 2685
Omura, Y., Heikkila, W. J., Umeda, T., Ninomiya, K., & Matsumoto, H. 2003, Journal of Geophysical Research (Space Physics), 108, 1197
Onofri, M., Isliker, H., & Vlahos, L. 2006, Physical Review Letters, 96, 151102
Petkaki, P., & Freeman, M. P. 2008, ApJ, 686, 686
Petkaki, P., Watt, C. E. J., Horne, R. B., & Freeman, M. P. 2003, Journal of Geophysical Research (Space Physics), 108, 1442
Poletto, G., & Kopp, R. A. 1986, in The Lower Atmosphere of Solar Flares; Proceedings of the Solar Maximum Mission Symposium, Sunspot, NM, Aug. 20-24, 1985 (A87-26201 10-92). Sunspot, NM, National Solar Observatory, 1986, (DOE-sponsored research.), ed. D. F. Neidig, 453
Pritchett, P. L. 2006, Geophys. Res. Lett., 33, L13104
Pritchett, P. L. 2008, Physics of Plasmas, 15, 102105
Schmitz, H., & Grauer, R. 2006, Journal of Computational Physics, 214, 738
Speiser, T. W. 1965, J. Geophys. Res., 70, 4219
Sui, L., Holman, G. D., & Dennis, B. R. 2004, ApJ, 612, 546
Sui, L., Holman, G. D., & Dennis, B. R. 2007, ApJ, 670, 862
Suzuki, A., & Shigeyama, T. 2010, Journal of Computational Physics, 229, 1643
Vlahos, L., Isliker, H., & Lepreti, F. 2004, ApJ, 608, 540
Wang, R., Lu, Q., Du, A., & Wang, S. 2010a, Physical Review Letters, 104, 175003
Wang, R., Lu, Q., Huang, C., & Wang, S. 2010b, Journal of Geophysical Research (Space Physics), 115, A01209
Wang, R., Lu, Q., Li, X., Huang, C., & Wang, S. 2010c, Journal of Geophysical Research (Space Physics), 115, A11201
Watt, C. E. J., Horne, R. B., & Freeman, M. P. 2002, Geophys. Res. Lett., 29, 1004
Wu, G. P., & Huang, G. L. 2009, A&A, 502, 341
Wu, G.-P., Huang, G.-L., & Tang, Y.-H. 2005, ChJAA (Chin. J. Astron. Astrophys.), 5, 99
Wu, G., Huang, G., & Ji, H. 2010a, ApJ, 720, 771
Wu, G.-P., Huang, G.-L., & Ji, H.-S. 2010b, RAA (Research in Astronomy and Astrophysics), 10, 1186
Yamada, M. 2011, Space Sci. Rev., 160, 25
Yang, Y.-H., Cheng, C. Z., Krucker, S., & Hsieh, M.-S. 2011, ApJ, 732, 15
Yokoyama, T., & Shibata, K. 1994, ApJ, 436, L197